The gene expression signature of electrical stimulation in the human brain

Snehajyoti Chatterjee[1,2], Yann Vanrobaeys[1#], Annie I Gleason[3#], Brian J. Park[4], Shane A. Heiney[1,2,5], Ariane E. Rhone[4], Kirill V. Nourski[4], Lucy Langmack[1,2], Budhaditya Basu[1,2], Utsav Mukherjee[1,2], Christopher K. Kovach[4,6], Zsuzsanna Kocsis[4,7], Yukiko Kikuchi[7], Yaneri A. Ayala[4], Christopher I. Petkov[4,7], Marco M. Hefti[8], Ethan Bahl[3], Jacob J Michaelson[3], Hiroto Kawasaki[4], Hiroyuki Oya[4], Matthew A. Howard III[4], Thomas Nickl-Jockschat[1,2,3,9,10,11], Li-Chun Lin[1,2,12], Ted Abel[1,2,3*]

Affiliations:

[1]Department of Neuroscience and Pharmacology, Iowa Neuroscience Institute, Carver College of Medicine, University of Iowa, Iowa City, IA, USA

[2]Iowa Neuroscience Institute, University of Iowa, Iowa City, IA, USA

[3]Department of Psychiatry, University of Iowa Hospitals and Clinics, Iowa City, IA, USA

[4]Department of Neurosurgery, University of Iowa Hospitals and Clinics, Iowa City, IA, USA

[5]Neural Circuits and Behavior Core, Iowa Neuroscience Institute Carver College of Medicine, University of Iowa, Iowa City, IA, USA

[6]Department of Neurosurgery, University of Nebraska Medical Center, Omaha, NE, USA

[7]Biosciences Institute, Newcastle University Medical School, Newcastle upon Tyne, UK

[8]Department of Pathology, University of Iowa Hospitals and Clinics, Iowa City, IA, USA

[9]Department of Psychiatry and Psychotherapy, Otto-von-Guericke University, Magdeburg, Germany

[10]German Center for Mental Health (DZPG), partner site Halle-Jena-Magdeburg, Germany

[11]Center for Intervention and Research on adaptive and maladaptive brain Circuits underlying mental health (C-I-R-C), Halle-Jena-Magdeburg, Germany

[12]Iowa NeuroBank Core, Iowa Neuroscience Institute, Carver College of Medicine, University of Iowa, Iowa City, IA, USA

[#]Authors contributed equally

*Corresponding author:

ted-abel@uiowa.edu

Keywords: Microglia, anterior temporal neocortex, direct electrical stimulation, single nuclei multiomics

Abstract

Direct electrical stimulation has been used for decades as a gold standard clinical tool to map cognitive function in neurosurgery patients[1-8]. However, the molecular impact of electrical stimulation in the human brain is unknown. Here, using state-of-the-art transcriptomic and epigenomic sequencing techniques, we define the molecular changes in bulk tissue and at the single-cell level in the human cerebral cortex following direct electrical stimulation of the anterior temporal lobe in patients undergoing neurosurgery. Direct electrical stimulation surprisingly had a robust and consistent impact on the expression of genes related to microglia-specific cytokine activity, an effect that was replicated in mice. Using a newly developed deep learning computational tool, we further demonstrate cell type-specific molecular activation, which underscores the effects of electrical stimulation on gene expression in microglia. Taken together, this work challenges the notion that the immediate impact of electrical stimulation commonly used in the clinic has a primary effect on neuronal gene expression and reveals that microglia robustly respond to electrical stimulation, thus enabling these non-neuronal cells to sculpt and shape the activity of neuronal circuits in the human brain.

Main

Electrical stimulation of the human brain has become an indispensable clinical tool for diagnosis and therapy[1-8]. In neurosurgical patients, cortical stimulation is the gold standard diagnostic tool to identify the location of functionally relevant brain regions that are critical for speech, language, or motor function[9,10] to avoid potential damage to these regions during surgery. Transient changes in gene expression underlie the ability of the brain to adapt to changes in the environment or brain perturbation, such as electrical stimulation. Dynamic transcriptomic patterns are essential for cognition[11-13], affective processing[14], addiction[15], and the initiation of behaviors[16,17]. Thus, electrical stimulation likely exerts neural effects via alterations in gene expression. Although diagnostic and therapeutic brain stimulation is conducted daily in thousands of patients worldwide, the molecular impact of electrical stimulation in the human brain remains unknown. Recent advances in molecular sequencing techniques have revolutionized transcriptomics by enabling mapping of changes in transcription and chromatin accessibility in single cells[18]. However, these experiments have only been conducted in rodents[19,20] and neurons derived from human induced pluripotent stem cells[21]. A recent pioneering study utilized a single nuclei molecular approach to link human brain transcriptomics signatures with oscillatory signatures of memory consolidation in epileptic patients undergoing an episodic memory task, but these gene expression measures were obtained many days after assessment of intracranial recording data during the task[22,23]. Therefore, research is needed to evaluate the more immediate effects on single-cell early gene expression, such as tens of minutes after neural system perturbation with electrical stimulation. Studies investigating gene expression profiles after electrical stimulation are particularly difficult to perform in human brains due to the requirement that tissue is sampled at precise temporal windows before and after stimulation.

Here, in patients undergoing clinical neurosurgical resection of pathological epileptogenic sites in the mesial temporal lobe, samples from tissue in the anterior

temporal lobe (ATL) that required clinical resection to access the deeper epileptogenic site for treatment were obtained before and after electrical stimulation. By analyzing gene expression at baseline and minutes after stimulation from the same patient, along with our analysis of samples taken from patients that did not receive electrical stimulation, we are able to distinguish genes responsive to electrical stimulation from the genes altered nonspecifically by surgical or disease-based factors that would be stable across samples. Our parameters for electrical stimulation were based on those regularly used in clinical mapping[24,25]; moreover, we referenced the human results to a similar electrical stimulation paradigm in mice, revealing a similar transcriptional profile. Finally, using a single-nuclei multi-omics approach, we provide insight into the cell-type-specific transcriptomic and epigenomic responses to electrical stimulation in the human brain, highlighting important effects beyond neurons, including microglia. This study provides fundamental insights into changes in cell-type specific molecular signatures in the human cortex after electrical stimulation, laying the groundwork for a molecular understanding of the impact of this fundamental tool in clinical neurosurgery, diagnosis, and treatment.

Results

We recruited eight adult neurosurgical patients undergoing surgical resection of seizure foci following clinical monitoring to treat epilepsy. The patients provided informed consent to take part in this research and were informed that tissue samples would only be taken from tissue that would require clinically resection for treatment. The patient participants underwent an anterior temporal lobectomy for access to a medial temporal lobe epileptogenic site, during which samples were resected from the neocortex and processed immediately after removal. The participants were evenly distributed between two experimental paradigms. In the first group with the electrically stimulated paradigm (4 participants), a baseline tissue sample was resected from the ATL after the craniotomy and durotomy, exposing the temporal lobe. Then, an adjacent region of the cortex was stimulated using a stimulation protocol commonly used for bipolar electrical stimulation (50 Hz) for 2 minutes[24,25] And resected approximately thirty minutes later (32.5 ± 11.2 min), a sample was taken from the stimulated region **(Fig. 1a; Supplementary Fig. 1a, Supplementary data 1).** In the second group with the

unstimulated paradigm (4 participants), a sample was taken at baseline, and then a second sample was taken without stimulation about 30 minutes later (37.3 ± 12.5 mins, **Fig. 1b; Supplementary Fig. 1a)**. The pre-stimulation sample and the unstimulated paradigm groups serves as controls for changes in baseline gene expression and changes in gene expression occurring as a result of the surgical procedure. Among the 8 participants, five were under general anesthesia, whereas three participants were awake during the surgical procedure. All the resected tissue samples from both the stimulated and unstimulated paradigms were taken well outside the seizure focus (27.8 ± 7mm from the border of seizure focus**, Supplementary Fig. 1b**).

Tissue samples were first subjected to bulk whole-transcriptome RNA sequencing (RNA-seq) to identify differentially expressed genes following electrical stimulation. Bulk RNA-seq analysis from the stimulated and corresponding baseline samples revealed 124 differentially expressed genes following electrical stimulation, with 112 up-regulated and 12 down-regulated genes **(Fig. 1c**; **Supplementary data 2)**. Enrichment network analysis was used to identify the pathways most represented among the differentially expressed genes in the stimulated paradigm. The top significant pathways were enriched with genes involved in cytokine activity, DNA-binding transcription activator activity (RNA Pol II), cytokine receptor binding, DNA-binding transcription activator activity, nuclear glucocorticoid receptor binding, chemokine activity, CCR chemokine receptor binding, RNA pol II specific DNA binding, chemokine receptor binding, and protein phosphatase activity **(Fig. 1d).** Notably, these genes were not significantly enriched for previously identified genes induced in regions showing seizure activity in the human brain **(Supplementary Fig. 2)**[26].

Bulk RNA-seq analysis from the unstimulated paradigm comparing unstimulated samples with corresponding baseline samples identified differential expression of only 16 genes, with nine up-regulated and seven down-regulated genes **(Fig. 1e, Supplementary data 3).** Only one gene, *NR4A3*, was found to be differentially expressed in both the stimulated and unstimulated groups **(Fig. 1g).** The lack of overlap between the differentially expressed genes observed in our stimulated and unstimulated groups suggests that the changes in gene expression that we see following electrical

stimulation do not reflect disease state or surgical effects such as craniotomy, brain temperature, and anesthesia, but reflect changes due to electrical stimulation.

We used a similar electrical stimulation paradigm in the mouse non-primary auditory cortex to investigate whether these gene expression changes are unique to human samples and to determine whether they are related to disease state [26,27]. Bulk RNA-seq was performed from samples collected 30 minutes following electrical stimulation and unstimulated samples collected at the same time from the contralateral side (**Fig. 2a**). Bulk RNA-seq identified 44 upregulated and 107 downregulated genes (**Fig. 2b, Supplementary data 4**). Pathway analysis identified from the upregulated genes were enriched for cytokine activity, chemokine activity, cytokine receptor binding, and CCR chemokine receptor binding. (**Fig. 2c**). We also found upregulated pathways linked to transcription and post-transcription regulatory pathways, such as mRNA 3'-UTR binding, mRNA3'-UTR AU-rich region binding, and transcription co-repressor activity. Comparing the stimulation-responsive genes from human bulk RNA-seq and mouse bulk RNA-seq revealed a significant correlation (R^2=0.0415, p-value <0.00001), especially cytokine-related genes were commonly upregulated following electrical stimulation in both humans and mice (**Fig. 2d**). Some of the pathways commonly altered by electrical stimulation between humans and mice are cytokine activity, chemokine activity, chemokine receptor binding, cytokine receptor activity, and the CCR chemokine receptor binding. Some common genes enriched in these chemokine and cytokine-related pathways are *CCL3*, *CCL4*, *CXCL1*, *IL1A*, and *TNF*. We further validated the expression of the cytokine activity-related genes *Ccl3* and *Ccl4* using qPCR analysis from mouse brain following electrical stimulation (**Fig. 2e**). The differentially expressed genes following electrical stimulation in the human cortex correlated significantly with learning-induced genes in the mouse cortex (R^2=0.2027, p-value <0.00001). Immediate early genes such as *Arc*, *Fos*, *Egr1*, *Nr4a1*, and *FosB* were upregulated in both datasets **(Supplementary Fig. 3)**. However, learning did not induce expression of cytokine activity related genes in mouse cortex. Thus, our findings of gene expression signature in response to electrical stimulation in the human and mouse brain reveal a molecular signature that partially conserved across species.

Next, we investigated the cell types exhibiting differential gene expression following electrical stimulation in the human brain by utilizing single nuclei multiomics (RNA and ATAC) on samples from the stimulated paradigm from 3 participants (**Fig 3a, Supplementary Fig. 4**). Cell clustering analysis identified seven major cell types in our samples—excitatory neurons, microglia, VIP-Sncg-Lamp5 inhibitory neurons, PValb-Sst inhibitory neurons, oligodendrocytes, oligodendrocytes precursor cells (OPC), and astrocytes (**Fig. 3b**). To determine the differentially expressed genes in each cell type following electrical stimulation, we performed a pseudobulk RNA-seq analysis due to its superior performance for detecting differential expression in single-cell RNA-sequencing analyses [28] and the stringent nature of this analysis. The pseudobulk analysis revealed that the microglia displayed the highest differential gene expression of all cell types with 31 upregulated genes (**Fig. 3c, Supplementary data 5**). Genes related to cytokine activity (*CCL3*, *CCL4*, *CCL3L1*, and *IL1B*,) were upregulated exclusively within microglia. Five genes were upregulated in oligodendrocytes (*FOS*, *HSPA1A*, *JUNB*, *GADD45B*, and *FOSB*), and only two genes were differentially expressed (one upregulated: *LHFPL3*, and one downregulated: *ROBO2*) in astrocytes (**Supplementary data 5**). Surprisingly, no differentially expressed genes were detected within the neuronal cell types (excitatory and inhibitory neuronal cell types). Comparing the upregulated genes in microglia with human and mice bulk RNA seq revealed 5 genes (*Fos*, *Dusp1*, *Ccl3*, *Ccl4*, *Zfp36*) that are commonly upregulated following electrical stimulation (**Fig. 3d**). *Atf3*, *Cd83*, *Egr3*, *Nr4a1*, *Il1b*, *Mcl1*, *Nedd9*, *Spp1*, *Nfkbid*, *Rgs1*, and *Ccl3l1* were found to be human microglia-specific genes induced by electrical stimulation that do not change in the mice cortex (**Fig 3d**). Pathways enriched among the upregulated genes in microglia included cytokine-related pathways such as cytokine activity, chemokine activity, CCR chemokine receptor, and cytokine receptor binding (**Fig. 3e**). Microglia exhibited activation of transcription regulatory pathways such as DNA-binding transcription activator activity and RNA polymerase-specific DNA binding TF binding (**Fig. 3e**). These results reveal that electrical stimulation increases the expression of genes that are involved in cytokine activity and transcription regulation in microglia.

To investigate if electrical stimulation has an impact on the epigenome, we assessed chromatin accessibility using the single nuclear assay for transposase-accessible chromatin with sequencing (snATAC-seq)[29] on human samples from the stimulated paradigm. We focused on promoter accessibility (-2 to +2 kb from TSS) to analyze changes in chromatin accessibility in snATAC-seq data (**Supplementary data 6**). The differentially accessible regions that were either enriched or depleted following electrical stimulation in microglia significantly correlated (R^2=0.0262, p-value<0.002) with the microglia gene expression from snRNA-seq (**Fig. 3f**), suggesting that the genes that exhibit induced expression following electrical stimulation also exhibit increased chromatin accessibility. Genes related to transcription regulators, such as NR4A1 and FOS, showed a positive correlation between transcriptome and chromatin accessibility. We also found enriched promoter accessibility and increased gene expression for CCL4 in microglia following electrical stimulation (**Fig 3g**). A recent study demonstrated that ambient RNA from neurons may contaminate non-neuronal cells in single-nuclei transcriptomic data[30]. Our snRNA seq data revealed the upregulation of several IEGs, such as *FOS*, *EGR3*, *JUNB,* and *NR4A1* within microglia. These genes are often seen to be upregulated in neurons following neuronal activation. However, our snATAC-seq data from the same samples also showed increased chromatin accessibility in microglial populations within IEG promoters, thus suggesting that the microglia-specific IEG expression is not due to neuronal ambient RNA contamination. Lastly, we analyzed genome-wide transcription factor (TF) binding motifs from the upregulated peaks following electrical stimulation in microglia using chromatin accessibility data. Genomewide TF motif analysis revealed enrichment of binding motifs for ELK3, ELK1, YY2, NRF1, HINFP, and ELK4 (**Fig. 3h, Supplementary data 7**). Interestingly, ELK4, a transcription factor downstream of MAPK signaling, is predicted to positively regulate the expression of *Ccl3* and *Ccl4*[31]. Thus, our sn-ATAC-seq results reveal a signature of transcription factor motifs and chromatin accessibility underlying electrical stimulation-induced gene expression in human microglia.

Our experimental design included internal controls (baseline/unstimulated samples) from each participant, enabling us to investigate the impact of electrical stimulation across individual participants. Therefore, we next examined the cell type-specific

response to electrical stimulation from within participants using our newly developed deep-learning computational tool, NEUROeSTIMator[32], to map the active population of cells following electrical stimulation in each participant, comparing stimulated samples with corresponding baseline controls. We estimated cell activity from the single nuclei RNA data from individual populations of cells with either baseline or stimulated from each participants (**Fig. 4a**). We used paired linear regression with bootstrap sampling to assess differences in estimated activity between conditions for each cell type (**Fig. 4b**). Interestingly, we observed that the microglial cluster showed a significant increase in activity scores following stimulation, and this effect was consistent across all three participants [β = 0.100301, p-value < 2e-16] (**Fig. 4c**). This data supports our bulk RNA seq and snRNAseq data. However, we observed variability in electrical stimulation-mediated activation of excitatory neurons across participants. We detected significant differences in activity when using all three participants [β = -0.053920, p-value < 2e-16]. One pair of samples showed a significant increase in activity [β = 0.032528, p-value = 0.000807], while 2 out of 3 pairs showed a significant decrease in activity [β = -0.022086, -0.083254, p-values = 1.58e-8, 4e-9] (**Fig. 4c**). Variability in activity estimates was also observed in inhibitory neuronal sub-types across participants (**Fig. 4c**).

To further investigate the epigenomic signature of cellular activity following electrical stimulation, we estimated activity from snATAC-seq data using a similar approach (**Fig. 5a**). Activity was estimated for cells using gene-level counts in promoter regions and paired linear regression with bootstrap sampling was used to assess activity between baseline and electrical stimulation (**Fig. 5b**). Consistent with the transcriptomics data, microglia showed a significant increase in promoter-informed activity estimates, and this effect was consistent across all three participants [β = 0.060977, p-value < 2e-16] (**Fig. 5c**). Neuronal clusters showed variability in activation in activity when considering all three participants [$\beta_{Excitatory}$ = 0.016163, $p\text{-value}_{Excitatory}$ = 0.000247; $\beta_{Inhibitory}$ = 0.028302, $p\text{-value}_{Inhibitory}$ = 2.283e-7]. Only one participant showed a significant increase in the excitatory[β = 0.04712, p-val = 0.000314] and inhibitory neurons (Sst-Pvalb) [β = 0.08863, p-value = 0.00201]. These findings suggest that microglia exhibit robust transcriptional and epigenomic responses to electrical stimulation and that neuronal cell types exhibit greater variability between patient participants.

Discussion

Electrical stimulation is a model for studying the human cortex with protocols that are used clinically for mapping the function of specific brain regions. Here, we take a molecular approach, defining the transcriptomic and epigenomic signatures of electrical stimulation at the single cell level in the human cortex in neurosurgical patient participants. Researchers have correlated human brain transcriptomics with prior recorded oscillatory signatures of memory consolidation[22,33], but have not previously examined the changes in gene expression that are rapidly and directly driven by electrical stimulation. Most work thus far has emphasized the role of neurons in responding to external stimuli, but our work reveals the critical role of microglia in sculpting the activity and function of brain circuits. In microglia, genes related to cytokine signaling showed the greatest induction pattern, and this was conserved across species. As previously hypothesized, we observed the induction of activity-dependent genes in our bulk RNA sequencing results, but to our surprise, single nuclei multiomics experiments revealed pronounced microglia-specific transcriptomic activation following electrical stimulation that was supported by analysis using NEUROeSTIMator[32], a deep-learning computational model. Identifying a microglial transcriptomic response following electrical stimulation represents an important conceptual advance in our understanding of the impact of this common form of electrical stimulation used clinically.

Microglia are critical modulators of neuronal function, acting to suppress excessive activity by inhibiting surrounding neurons, including excitatory neurons[34]. Although classified as non-excitable cells, microglia exhibit electrophysiological stimulus-response features, and changes in their membrane potential affect crucial microglial functions including phagocytosis, chemotaxis, and cytokine release[35]. Our analyses identified critical molecular components within microglia that change with electrical stimulation, including chemokine-encoding genes such as *CCL3* and *CCL4*, which act to alter microglial motility, influence neuronal-microglial interactions, and shape neuronal connectivity[34,36-39]. These chemokines are ligands for C-C chemokine receptor type 5 (CCR5), which regulates neuronal excitability and memory allocation in the hippocampus[40]. Previous rodent studies have shown that neuronal activation using

chemogenetic approaches leads to distinct gene expression changes in microglia, including genes encoding chemokines[34]. Our work also revealed that genes encoding transcription factors such as FOS and NR4A1 are induced in microglia in response to electrical stimulation. Further, we observed increased promoter accessibility at these genes, underscoring the conclusion that these genes are transcriptionally upregulated in microglia after stimulation and broadening the potential functional impact of these immediate early genes beyond their more frequently studied role in neurons. Indeed, NR4A1 acts in neurons as a transcription factor essential for memory consolidation[41,42] and functions in microglia as a molecular rheostat, contributing to the maintenance of a threshold that prevents microglial activation[43]. Furthermore, our study of chromatin accessibility defines a cell-type-specific signature of transcriptional motifs driving these processes that includes motifs for ELK4 and NRF1, which have been identified in other studies as transcriptional motifs associated with the differential regulation of molecular pathways in specific subsets of microglia[44,45].

This study represents a rare opportunity to define the molecular impact of electrical stimulation in patients undergoing anterior temporal lobectomy due to therapy refractory seizures. Although presenting a unique opportunity, it is important to note the caveats that come from this research carried out in a setting focused on clinical efficacy in patients that have epilepsy. Thus, we can not control all of the parameters as we might in an experiment carried out in a model organism, although we have worked to address three potential limitations of our study. First, our experimental design includes a group that does not receive electrical stimulation, thus controlling for the impact of the surgical procedure, craniotomy, brain temperature changes, and levels of anesthesia when present. We also show that electrical stimulation in a mouse model, in which we can control many additional parameters, gives rise to similar molecular changes. Importantly, our mouse experiment included the use of an inactive electrode, thus controlling for mechanically induced changes in gene expression. Second, the stimulation pattern used is safe and efficacious for brain mapping in human patients but is not optimized to modulate activity in specific circuits and cell types in the brain. Indeed, the stimulation protocol used leads to the functional disruption of brain regions[1], and thus, we may expect to see reductions in activity-dependent gene expression in

337 excitatory neurons, as seen in two patients in our NEUROeSTIMator analysis. Third, it
338 goes without saying that these patients have severe therapy refractory epilepsy.
339 However, the resected samples were taken a considerable distance from the seizure
340 foci (see Suppl. Fig. 1b), our gene induction signatures do not resemble those seen in
341 actively spiking tissue[26], and our molecular changes are seen in a mouse model that
342 does not exhibit seizures.

343 Despite these caveats, we were able to identify a reliable cell-specific signature of the
344 impact of electrical stimulation in the living human brain. This study demonstrates for the
345 first time a unique transcriptomic and epigenomic signature in microglia following direct
346 electrical stimulation, representing a conceptual advance in our understanding of how
347 the brain responds to an important clinical tool used to map brain function. These
348 findings have the potential to inform the clinical practice of diagnostic and therapeutic
349 brain stimulation. Clinical and translational research has focused mainly on the
350 immediate effects of stimulation in neuronal populations, while microglia receive little
351 attention, often being discussed with regard to neuroimmunological aspects[46]. Although,
352 for clinical mapping, clinicians rely on the immediate neuronal effects on behavior (e.g.,
353 speech arrest), there is growing evidence that therapeutic effects of electrical
354 stimulation can accumulate gradually over time[47]. We could not test a range of
355 stimulation frequencies and intensities or examine a broad range of brain areas
356 because of clinical limitations, but our results raise the intriguing hypothesis that
357 microglia, not just neurons, shape plasticity after repetitive stimulation. Our work further
358 highlights that cytokine and chemokine-based mechanisms enable microglia to respond
359 to electrical stimulation and sculpt circuit function, making these potential targets to
360 modify circuit activity with pharmacological approaches. Microglia exist in different
361 subpopulations depending on transcriptional state and age[48,49], and our epigenetic work
362 has revealed particular transcriptional motifs that mark microglial subtypes important for
363 cortical plasticity. It will be especially interesting in future work to extend our studies to
364 stimulation protocols used therapeutically as well as natural stimuli to probe the critical
365 role of microglial signaling in mediating the response of the human brain to experience.

366 **Acknowledgments**

We thank Rashmi N. Mueller who oversaw anesthesia to manage pain levels before, during, and after surgical procedures, and Kyle S. Conway for helping with the initial pathological assessment. We thank the Iowa Institute of Human Genetics (IIHG) core for RNA seq library preparation and sequencing.

Funding: This work was supported by grants from the National Institute of Health R01 MH 087463 to T.A and The University of Iowa Hawkeye Intellectual and Developmental Disabilities Research Center (HAWK-IDDRC) P50 HD103556 to T.A., The National Institute of Health R00 AG068306 to S.C. and the National Institute of Health R01 DC004290 to M.A.H., National Science Foundation BCS-2342847 to C.I.P. T.N.J & C.I.P. are supported by a Research Program of Excellence of the Carver Trust and the Iowa Neuroscience Institute. T.A. is supported by the Roy J. Carver Chair of Neuroscience, JMM is supported byt the Roy J. Carver Professor of Neuroscience and the Andrew H. Woods Professorship supported T.N.J. The Neural Circuits and Behavior Core as well as the NeuroBank Core are supported by the Roy J. Carver Charitable Trust.

Author contributions

S.C., M.A.H., and T.A. conceived the project, designed the experiments, and interpreted the data. S.C. and T.A. wrote the manuscript with assistance from C.I.P., L.L., and T.N.J., and inputs from other co-authors. H.K. performed human surgery and electrical stimulation and resected the tissue. A.E.R and C.K.K. processed with IRB and MRI imaging registration. H.O, M.A.H, T.N-J, and K.V.L provided advice on surgical procedures and electrical stimulation. M.M.H. provided a pathological assessment. L.C.L., K.V.N., and B.J.P. collected the tissue and images during resection. S.C., B.J.P., L.C.L., U.M., L.L. performed human or mouse tissue samples experiments. C.I.P. and Y.A.A. performed distance to the seizure site analysis. U.M. and L.L. performed mouse brain imaging and data analysis. Y.V., A.I.G., and B.B. performed the bioinformatics analysis with inputs from E.B. and J.J.M. S.A.H. performed the mouse surgery and electrical stimulation experiments. K.V.N, C.K.K, Z.K. Y.K, C.I.P, M.H, J.J.M, E.B, U.M, and T.N.J. provided input on data analysis and interpretation. All authors discussed the results and commented on the manuscript.

Competing interests

T.A. is a scientific advisor to Aditum Bio and Radius Health and serves on the scientific advisory board of Embark Neuro. The other authors declare no conflicting interests.

Figure legends

Figure 1. **Electrical stimulation of the human cortex induces changes in genes associated with cytokine activity and transcription regulation. a, b**. Schematics of stimulated (**a**) and unstimulated (**b**) paradigms in the human anterior temporal lobe. For both paradigms sample A was taken at T = 0 minutes then an adjacent sample B was taken at either 30 min after stimulation (**a**, stimulated paradigm, 4 participants) or 30 min after sample A was taken (**b**, unstimulated paradigm, 4 participants). **c.** Volcano plot showing gene expression changes in the stimulated samples. The most significant genes (FDR < 0.05) are labeled in red (upregulated) or blue (downregulated). **d.** Cnet plot showing pathway enrichment analysis of the genes significantly (FDR < 0.05) differentially expressed in the stimulated samples. **e**. Volcano plots showing gene expression changes in the unstimulated samples. The most significant genes (FDR < 0.05) are labeled in red (upregulated) or blue (downregulated).

Figure 2. Electrical stimulation of mouse cortex induces changes in genes associated with cytokine activity and transcription regulation. a. The mouse auditory cortex was stimulated, tissue was collected 30 min later, and the contralateral auditory cortex was obtained as baseline control. **b.** Volcano plot showing gene expression changes after stimulation. The most significant genes (FDR < 0.05) are labeled in red (upregulated) or blue (downregulated). **c.** Cnet plot showing pathway enrichment analysis of the genes significantly (FDR < 0.05) affected by electrical stimulation. **d.** Quadrant plot comparing genes induced by electrical stimulation in mice with genes induced by electrical stimulation in human brain. Genes upregulated in both mice and human brains after stimulation are labeled. The size, opacity, and color intensity of each data point denotes the minimum false discovery rate value for a gene between each transcriptomic datasets. **e.** qPCR analysis of the genes related to cytokine activity comparing stimulated versus baseline controls in mice cortex. n=7/group.

Figure 3. Single nuclei multiomics reveal cell type-specific transcriptomic and epigenomic changes following electrical stimulation. a. Single nucleus multiomic experimental approach. **b.** UMAP shows the specific cell types from each cluster. **c.** Volcano plot showing differentially expressed genes in microglia using pseudobulk analysis comparing stimulated vs baseline samples from human brain (FDR<0.1). **d.** Upset plot comparing DEGs in mouse, human bulk RNA seq, and human microglia snRNA-seq after electrical stimulation. **e.** Cnet plot showing pathway enrichment analysis of the genes significantly (FDR < 0.1) affected by electrical stimulation in human microglia. **f.** Quadrant plot comparing DEGs from snRNA-seq following electrical stimulation in human microglia and genes with open chromatin accessibility from snATAC-seq in microglia following electrical stimulation. Genes upregulated in both mice and human brains after stimulation are labeled. **g**. Quadrant plot comparing gene expression changes (log10(FDR)*log2fold-change) between snRNA-seq (x-axis) and snATAC-seq (y-axis) data in microglia after stimulation. Genes in red in the top-right corner of the plot are significantly upregulated at the gene expression level and exhibit increased chromatin accessibility. The dotted lines represent FDR thresholds of 0.01. The dashed line represents the linear regression applied to this quadrant plot. **g.** DNA motifs are overrepresented in the set of peaks differentially accessible in microglia after stimulation. Motifs are ranked based on significance from the most significant left to right. **h.** The coverage plot shows ATAC peaks at the CCL4 locus. Each track represents a normalized chromatin accessibility signal from the ATAC assay for each cell type and condition (baseline or stimulated).

Figure 4. NEUROeSTIMator for snRNA-seq. Cell-type specific differences in activity estimates. a. UMAP of cells representing the activity estimated from the RNA gene counts in the baseline and stimulated conditions. Darker blue points are cells with higher estimated activity. **b.** The bootstrap distribution of the difference between activity estimates (stimulated – baseline) by cell type. Horizontal bars indicate the 95% confidence interval of the mean difference in activity estimate. **c.** Activity estimates in selected cell types in baseline (green) and stimulated (orange) conditions.

Figure 5. NEUROeSTIMator for snATAC-seq. Cell-type specific differences in activity estimates. a. UMAP of cells representing the activity estimated from the ATAC

counts in the baseline and stimulated conditions. Darker blue points are cells with higher estimated activity. **b.** The bootstrap distribution of the difference between activity estimates (stimulated – baseline) by cell type. Horizontal bars indicate the 95% confidence interval of the mean difference in activity estimate. **c.** Activity estimates in selected cell types in baseline (green) and stimulated (orange) conditions.

Materials and Methods:

Patient participants: The study participants were 8 adult neurosurgical patients (6 female, 2 male, age 19-63 years old, median age 41 years old) with medically refractory epilepsy. The patients were undergoing surgical resection of seizure foci following non-invasive electroencephalography (EEG) or invasive iEEG monitoring. All patients were diagnosed with intractable epilepsy. All patients underwent ATL resection surgery for epilepsy of various etiologies **(Extended data fig 1).**

Two of the patient participants, L472 had a cavernoma and L475 had a dysembryoplastic neuroepithelial tumor. X out of Y participants were required to be awake during the surgical resection, and the rest were anesthetized. All patient participants except #6 were non-smokers. Participant's age, sex, surgery, and awake or sedative information were recorded (**Extended Data Table 1)**. All participants were native English speakers, 7 were right-handed, 1 was left-handed, and all had left language dominance as determined by Wada tests. All participants underwent audiometric evaluation before the study, and none were found to have hearing deficits or word recognition scores deemed sufficient to affect the findings presented in this study. The vision was self-reported as normal or corrected to normal with glasses or contact lenses. As determined by standard neuropsychological assessments, cognitive function was in the average range in all participants. Research protocols were approved by the University of Iowa Institutional Review Board (IRB 201910791, 201911084) and the National Institutes of Health. Written informed consent was obtained from all participants.

Procedure: Surgery was performed awake, under general anesthesia or monitored anesthetic care. Standard craniotomy was performed by the same senior epilepsy neurosurgeon in all patients to reach the epilepsy focus for resection, which involved the

anterior and medial temporal lobe in all patients except one who had a temporal encephalocele and surrounding anterolateral temporal cortical focus. Before neurosurgical ATL resection, cortical tissue from the anterior temporal lobe was sampled by the neurosurgeon and handed over to the research team for analysis. The experimental condition was defined by an electrical “stimulation paradigm” and a control “no-stimulation paradigm**”**. The location of the sampled tissue is plotted on anatomic brain reconstructions **(Extended data fig 1).** The 30 minutes in between the control and experimental samples was clinically required for the clinical EEG team to record inter-ictal activity with surface recording grids placed gently on the brain surface.

There were 4 participants (1 iEEG and 3 EEG patients) who underwent the “stimulation paradigm” and 4 (2 iEEG and 2 EEG patients) who underwent the “no-stimulation paradigm” **(Extended Data Table 5)**.

In the “stimulation paradigm”, a baseline sample was obtained from the anterior temporal cortex that would be resected in the planned surgical resection. The area directly adjacent to where the baseline sample was collected was stimulated with direct bipolar electric stimulation (50 Hz frequency, 0.2 ms pulse duration, 2 min stimulation duration, and 10 V voltage). The stimulated area was then sampled after a period of 30 minutes to allow for gene expression[50,51]. In the “no stimulation paradigm”, no direct electric stimulation was performed and the area directly adjacent to the baseline sample was collected 30 minutes after initial baseline sampling.

After sampling the tissue samples were immediately placed in a sterile container on dry ice. The average weight of the baseline sample was 88.0 ± 33.2 mg (mean, standard deviation) and the adjacent sample was 113.4 ± 62.7 mg. After the collection of all samples in this fashion, they were weighed and transferred to a freezer at -80° C for storage until further testing.

Sample Localization to MNI space: All samples were from the same cortical region. Intraoperative photos of the sample sites were obtained during the time of surgery. Using patient participant matched preoperative T1 sequence MRI, the sample sites were mapped onto their anatomic brain reconstructions **(Extended data fig. 1)**. They were also mapped onto MNI space coordinates.

Human cortical tissue RNA extraction, library preparation, and sequencing: Total RNA was extracted from sampled human brains using miRNeasy Mini Kit (Qiagen, CA, USA). The tissue samples were homogenized in QIAzol (Qiagen, CA. USA) stainless steel beads (Qiagen, CA, USA). Chloroform was then used for phase separation. RNA containing an aqueous layer was further purified using the RNeasy MinElute spin column. RNA was finally eluted in RNase-free water. RNA concentrations were estimated using a Nanodrop (Thermo Fisher Scientific, MA, USA) and Qubit (Thermo Fisher Scientific, MA, USA). RNA libraries were prepared at the Iowa Institute of Human Genetics (IIHG), Genomics Division, using the Illumina Stranded Total RNA Prep, Ligation with Ribo-Zero Plus (Illumina Inc., San Diego, CA). The KAPA Illumina Library Quantification Kit (KAPA Biosystems, Wilmington, MA) was used to measure library concentrations. Pooled libraries were sequenced on Illumina NovaSeq6000 sequencers with 150-bp paired-end chemistry (Illumina) at the Iowa Institute of Human Genetics (IIHG) core.

Bulk RNA sequencing analysis: RNA-seq data were processed with the bcbio-nextgen pipeline (https://github.com/bcbio/bcbio-nextgen, version 1.2.9). The pipeline uses STAR[52] to align reads to the hg38 or mm10 reference genome and quantifies expression at the gene level with feature Counts [53]. All further analyses were performed using R. For gene-level count data, the R package EDASeq was used to account for sequencing depth (upper quartile normalization) [54]. Latent sources of variation in expression levels were assessed and accounted for using RUVSeq (RUVs mode using all features) [55]. Appropriate choice of the RUVSeq parameter k was guided through inspection of principal components analysis (PCA) plots. Specifically, the smallest value k was chosen where PCA plots demonstrated replicate sample clustering in the first three principal components[56]. Differential expression analysis was conducted using the edgeR package[57]. Codes to reproduce the RNA-seq differential gene expression analysis are available at https://github.com/YannVRB/Human-brain-stimulation.git.

All the transcriptomics data have been deposited in NCBI's Gene Expression Omnibus and are accessible through GEO Series accession number GSE224952.

Downstream pathway analysis:

548 The enrichment analysis of differentially expressed genes-associated pathways and
549 molecular functions from the stimulated and unstimulated RNA-seq was performed with
550 the Gene Ontology (GO–molecular function) databases using clusterProfiler package in
551 R. Only the pathways with an adjusted p-value < 0.05 were considered as significant
552 and displayed. Further, the enrichment data were visualized using 'cnetplot' function of
553 clusterProfiler.

554

555 ***Single-nuclei multiomics (nuclei isolation, library preparation, sequencing:*** Nuclei
556 were isolated from brain tissue using the Chromium Nuclei Isolation Kit (10X
557 Genomics). Briefly, frozen tissue was dissociated with pestle in lysis buffer, passed
558 through nuclei isolation column and spun at 16,000 rcf for 20 sec at 4^0C. Flowthrough
559 was vortexed and spun at 500 rcf for 3 mins at 4^0C. Pellet was resuspended with debris
560 removal buffer and centrifuged at 700 rcf for 10 mins at 4^0C, nuclei resuspended in
561 wash buffer and centrifuged again at 500 rcf for 5 mins at 4^0C. Pellet was resuspended
562 in resuspension buffer and nuclei were counted using a hemocytometer. Nuclei were
563 directly processed for droplet capture for single cell multiome ATAC + gene expression
564 using a chromium controller (10X Genomics). Chromium Next GEM Single Cell
565 Multiome ATAC + Gene v1 chemistry was used to create single nuclei ATAC and RNA
566 libraries from the same cell. Two baseline and two stimulated samples were used for
567 independent replicates. Libraries were sequenced on an Illumina Novaseq 6000 with a
568 150 bp paired end read setup.

569 ***Single-nuclei multiomic data processing and analysis:*** To analyze the RNA part of
570 the human brain stimulation multiomic data, gene counts were normalized and log
571 transformed (LogNormalize), and the top 2,000 most variable features between each
572 nuclei were identified using FindVariableFeatures (selection.method = 'vst'). Features
573 that are repeatedly variable across nuclei and datasets were selected for integration
574 (SelectIntegrationFeatures). We then identified anchors (FindIntegrationAnchors), which
575 took the list of 4 individual Seurat objects for each sample as input and used these
576 anchors to integrate the four datasets together (IntegrateData). The following analyses
577 were performed on the integrated Seurat object. Linear dimensionality reduction was

578 performed by principal component analysis (runPCA, npcs = 25). A k-nearest-
579 neighbors graph was constructed based on Euclidean distance in PCA space and
580 refined (FindNeighbors, npcs = 30), then nuclei were clustered using the Louvain
581 algorithm (FindClusters, resolution = 0.5). Clusters were visualized with UMAP
582 (runUMAP, dims = 30). Cell types were annotated by label transfer cell labels from an
583 existing human primary motor cortex reference dataset from the Allen Institute (doi:
584 10.1038/s41586-021-03465-8) (FindTransferAnchors and TransferData). Cell types
585 identification was validated by expression of specific biomarkers. Prior of running
586 differential gene expression analysis, as recommended by recent publications
587 (https://doi.org/10.1038/nmeth.4612 and https://doi.org/10.1038/s41467-020-19894-4),
588 we used an aggregation-based (pseudobulk) workflow. We aggregated all cells within
589 the same cell type and sample using the AggregateExpression function. This returns a
590 Seurat object where each 'cell' represents the pseudobulk profile of one cell type in one
591 individual. After we aggregated cells, we performed celltype-specific differential
592 expression between stimulated and baseline samples using DESeq2.

593 To analyze ATAC part of the human brain stimulation multiomic data, prior to integrating
594 the four Seurat object, the default assay was switched to ATAC, and peak calling was
595 performed. Since the set of peaks identified by Cellranger often merges distinct peaks
596 that are close together, creating a problem for motif enrichment analysis and peak-to-
597 gene linkage, we identified a more accurate set of peaks by calling peaks using MACS2
598 (CallPeaks) on all cells together. Peaks on nonstandard chromosomes and in genomic
599 blacklist regions were removed (keepStandardChromosomes and subsetByOverlaps).
600 Normalization was performed with a frequency-inverse document frequency
601 normalization which normalizes across cells and peaks (RunTFIDF). Then, a feature
602 selection was performed using all the peaks as input (FindTopFeatures). The
603 dimensional reduction was performed on the TF-IDF normalized matrix with the
604 selected peaks using a singular value decomposition (RunSVD). To mimic the open
605 chromatin conformation of a gene, a gene activity matrix was calculated using a window
606 of 1000bp before and after the transcription start site of each protein coding gene
607 (GeneActivity). Differentially accessible transcription start sites in individual clusters
608 between baseline and stimulated samples were calculated using a logistic regression

framework (FindMarkers, test.use = 'LR', latent.vars = 'nCount_peaks', Padj < 0.05). Motif and transcription factor enrichment analysis for Microglia cluster was performed using FindMotifs on genome-wide all peaks assay of the Seurat object. The top six enriched motifs in microglia cluster are shown. Genomic locations of typical genes like CCL4 were presented (CoveragePlot). It also includes co-accessibility between peaks and transcription start site of genes. Codes to reproduce the multiomic data analysis are available at https://github.com/YannVRB/Human-brain-stimulation.git.

NEUROeSTIMator analysis. Gene-level counts for each cell were used as input for the NEUROeSTIMator model [33] to estimate transcriptional signatures of cell activity. Activity was also estimated for cells using gene-level counts in promoter regions from the ATAC assay. Estimated activity was assessed for significant differences between the baseline and stimulated conditions across the donors and cell types using paired linear regression. P-values were adjusted for multiple testing with the Benjamini-Hochberg correction. To account for variable sample sizes across cell types and participants, bootstrap resampling was performed (n = 100 cells per donor, replicates = 1000) for each cell type in each condition to generate a distribution of the mean difference in estimated activity between conditions.

To account for variation in sample size across cell types and participants, bootstrap resampling was performed (n = 100 cells per participant, replicates = 1000) for each cell type of the mean difference in estimated activity scores between conditions (mean stimulated – mean baseline). The distributions were analyzed by mean and 95% confidence interval.

Animals: Adult male C57BL/6J mice were purchased from The Jackson Laboratory were 3 to 4 months of age during experiments. All mice had free access to food and water; lights were maintained on a 12-hour light/12-hour dark cycle.

Mouse electrical stimulation: Stimulation experiments were performed in anesthetized adult male C57BL6/J mice. Anesthesia was induced with 5% isoflurane by inhalation and maintained at 1.8-2% for the duration of the experiment. The mouse was placed in a stereotax (Kopf) and a midline incision was made and the skin retracted to expose the temporal muscle bilaterally. The dorsal insertion of both temporal muscles was

removed, and the muscles retracted. A 2-3 mm craniotomy was made over area AuV (centered at 2.9 mm posterior, 4.2 mm lateral, 2.8 mm ventral from Bregma based on Paxinos atlas) bilaterally to expose the cortical surface and a small square of gel foam soaked in ACSF was applied on top of the dura to prevent it from dehydrating. For each mouse the side of electrical stimulation and sham stimulation were alternated, with the sham side serving as the baseline control for gene expression profiling. Electrical stimulation was delivered through a bipolar ball electrode constructed from two silver wires in which the uninsulated tips were melted under a butane flame (1 mm tip size, 2 mm tip spacing). For both electrical and sham stimulations, the gel foam was removed and the electrode was gently lowered to make contact with the cortical surface. For electrical stimulation, a biphasic pulse train was then delivered for two minutes (8 mA, 50 Hz, 200 µs pulse width). For the sham stimulation no current was delivered but the electrode was left in place for 2 minutes. Following electrical or sham stimulation the electrode was slowly retracted, and the exposed dura was covered with gel foam. Selection for hemisphere was performed randomly, which resulted in the order of electrical and sham stimulation alternating from mouse to mouse. No more than 5 minutes elapsed between electrical or sham stimulation of both sides. After both sides were stimulated (electrical or sham) the mouse was left in the stereotax under anesthesia for 30 minutes before euthanasia and tissue collection. Tissue samples were immediately stored at -80^{0}C in RNA later solution (Ambion).

RNA extraction, cDNA preparation and qPCRs from mouse auditory cortex: Tissue samples were homogenized in Qiazol (Qiagen) using stainless steel beads (Qiagen). Chloroform was added and centrifuged at 12,000*g* at room temperature for 15 min to separate RNA in the aqueous phase. RNA was precipitated in ethanol and cleared using RNeasy kit (Qiagen). RNA eluted in nuclease-free water was then treated with DNase (Qiagen) at room temperature for 25 min to remove genomic DNA. RNA was further precipitated in ethanol, sodium acetate (pH 5.2) and glycogen overnight at −20°C. RNA was precipitated by centrifugation at 30,000g for 20 min, precipitate washed with 70% ethanol and the dried RNA pellet was resuspended in nuclease-free water. RNA concentration was measured using NanoDrop (Thermo Fisher Scientific). 1 µg of RNA was used for complementary DNA (cDNA) preparation using the SuperScript IV First-

Strand Synthesis System (Ambion). Real-time reverse transcription polymerase chain reactions (RT-PCRs) were performed on the QuantStudio 7 Flex Real-Time PCR System (Applied Biosystems, Life Technologies). Data were normalized to housekeeping genes (*Tubulin*, *Pgk1*, and *Actin*), and $2^{(-\Delta\Delta Ct)}$ method was used for gene expression analysis.

Mouse cortex spatial transcriptomics analysis (Yann): Spatial transcriptomics data were obtained from the Visium Spatial Gene Expression platform, as described previously[42]. This dataset provides comprehensive gene expression profiles across various brain regions, including the mouse cortex. To focus on the mouse auditory cortex, the closest homolog to the human anterior temporal lobe, we manually selected spatial spots from the Visium data corresponding to this brain region. This selection was based on anatomical landmarks and known spatial coordinates for the auditory cortex. For each of the 14 mice in the dataset, we subsetted the data to include only these selected spots, thereby isolating the gene expression profiles specifically from the auditory cortex.

The dataset of 14 mice was divided into two experimental conditions: 7 mice underwent Spatial Object Recognition after 1 hour (SOR-1h), while the other 7 mice were kept in their homecage environment without specific tasks. Based on the Visium spots data overlaying the mouse auditory cortex, differential gene expression analysis was performed to identify genes that were significantly differentially expressed between the SOR-1h and homecage conditions.

Statistics: For the qPCR analysis, the Wilcoxon matched pairs signed rank test and one sample Wilcoxon test was performed.

References

1 Penfield, W. & Rasmussen, T. Vocalization and arrest of speech. *Arch Neurol Psychiatry* **61**, 21-27 (1949). https://doi.org:10.1001/archneurpsyc.1949.02310070027002

2 Lozano, A. M. *et al.* Deep brain stimulation: current challenges and future directions. *Nat Rev Neurol* **15**, 148-160 (2019). https://doi.org:10.1038/s41582-018-0128-2

3 Okun, M. S. Deep-brain stimulation for Parkinson's disease. *N Engl J Med* **367**, 1529-1538 (2012). https://doi.org:10.1056/NEJMct1208070

4 De Risio, L. *et al.* Recovering from depression with repetitive transcranial magnetic stimulation (rTMS): a systematic review and meta-analysis of preclinical studies. *Transl Psychiatry* **10**, 393 (2020). https://doi.org:10.1038/s41398-020-01055-2

5 Kellner, C. H. *et al.* ECT in treatment-resistant depression. *Am J Psychiatry* **169**, 1238-1244 (2012). https://doi.org:10.1176/appi.ajp.2012.12050648

6 Krauss, J. K. *et al.* Technology of deep brain stimulation: current status and future directions. *Nat Rev Neurol* **17**, 75-87 (2021). https://doi.org:10.1038/s41582-020-00426-z

7 Sheth, S. A. & Mayberg, H. S. Deep Brain Stimulation for Obsessive-Compulsive Disorder and Depression. *Annu Rev Neurosci* **46**, 341-358 (2023). https://doi.org:10.1146/annurev-neuro-110122-110434

8 Goodman, W. K., Storch, E. A. & Sheth, S. A. Harmonizing the Neurobiology and Treatment of Obsessive-Compulsive Disorder. *Am J Psychiatry* **178**, 17-29 (2021). https://doi.org:10.1176/appi.ajp.2020.20111601

9 George, D. D., Ojemann, S. G., Drees, C. & Thompson, J. A. Stimulation Mapping Using Stereoelectroencephalography: Current and Future Directions. *Front Neurol* **11**, 320 (2020). https://doi.org:10.3389/fneur.2020.00320

10 Grande, K. M., Ihnen, S. K. Z. & Arya, R. Electrical Stimulation Mapping of Brain Function: A Comparison of Subdural Electrodes and Stereo-EEG. *Front Hum Neurosci* **14**, 611291 (2020). https://doi.org:10.3389/fnhum.2020.611291

11 Yap, E. L. & Greenberg, M. E. Activity-Regulated Transcription: Bridging the Gap between Neural Activity and Behavior. *Neuron* **100**, 330-348 (2018). https://doi.org:10.1016/j.neuron.2018.10.013

12 Sagar, S. M., Sharp, F. R. & Curran, T. Expression of c-fos protein in brain: metabolic mapping at the cellular level. *Science* **240**, 1328-1331 (1988). https://doi.org:10.1126/science.3131879

13 Guzowski, J. F., McNaughton, B. L., Barnes, C. A. & Worley, P. F. Environment-specific expression of the immediate-early gene Arc in hippocampal neuronal ensembles. *Nat Neurosci* **2**, 1120-1124 (1999). https://doi.org:10.1038/16046

14 Laricchiuta, D. *et al.* Optogenetic Stimulation of Prelimbic Pyramidal Neurons Maintains Fear Memories and Modulates Amygdala Pyramidal Neuron Transcriptome. *Int J Mol Sci* **22** (2021). https://doi.org:10.3390/ijms22020810

15 Bali, P. & Kenny, P. J. Transcriptional mechanisms of drug addiction☐*Dialogues Clin Neurosci* **21**, 379-387 (2019). https://doi.org:10.31887/DCNS.2019.21.4/pkenny

16 Fernandez-Albert, J. *et al.* Immediate and deferred epigenomic signatures of in vivo neuronal activation in mouse hippocampus. *Nat Neurosci* **22**, 1718-1730 (2019). https://doi.org:10.1038/s41593-019-0476-2

17 Marco, A. *et al.* Mapping the epigenomic and transcriptomic interplay during memory formation and recall in the hippocampal engram ensemble. *Nat Neurosci* **23**, 1606-1617 (2020). https://doi.org:10.1038/s41593-020-00717-0

18 Trevino, A. E. *et al.* Chromatin and gene-regulatory dynamics of the developing human cerebral cortex at single-cell resolution. *Cell* **184**, 5053-5069 e5023 (2021). https://doi.org:10.1016/j.cell.2021.07.039

19 Reijmers, L. G., Perkins, B. L., Matsuo, N. & Mayford, M. Localization of a stable neural correlate of associative memory. *Science* **317**, 1230-1233 (2007). https://doi.org:10.1126/science.1143839

20 Halder, R. *et al.* DNA methylation changes in plasticity genes accompany the formation and maintenance of memory. *Nat Neurosci* **19**, 102-110 (2016). https://doi.org:10.1038/nn.4194

21 Boulting, G. L. *et al.* Activity-dependent regulome of human GABAergic neurons reveals new patterns of gene regulation and neurological disease heritability. *Nat Neurosci* **24**, 437-448 (2021). https://doi.org:10.1038/s41593-020-00786-1

22 Berto, S. *et al.* Gene-expression correlates of the oscillatory signatures supporting human episodic memory encoding. *Nat Neurosci* **24**, 554-564 (2021). https://doi.org:10.1038/s41593-021-00803-x

23 Konopka, G. Cognitive genomics: Linking genes to behavior in the human brain. *Netw Neurosci* **1**, 3-13 (2017). https://doi.org:10.1162/NETN_a_00003

24 Berger, M. S. & Ojemann, G. A. Intraoperative brain mapping techniques in neuro-oncology. *Stereotact Funct Neurosurg* **58**, 153-161 (1992). https://doi.org:10.1159/000098989

25 Sanai, N., Mirzadeh, Z. & Berger, M. S. Functional outcome after language mapping for glioma resection. *N Engl J Med* **358**, 18-27 (2008). https://doi.org:10.1056/NEJMoa067819

26 Brueggeman, L. *et al.* Drug repositioning in epilepsy reveals novel antiseizure candidates. *Ann Clin Transl Neurol* **6**, 295-309 (2019). https://doi.org:10.1002/acn3.703

27 Altmann, A. *et al.* A systems-level analysis highlights microglial activation as a modifying factor in common epilepsies. *Neuropathol Appl Neurobiol* **48**, e12758 (2022). https://doi.org:10.1111/nan.12758

28 Murphy, A. E. & Skene, N. G. A balanced measure shows superior performance of pseudobulk methods in single-cell RNA-sequencing analysis. *Nat Commun* **13**, 7851 (2022). https://doi.org:10.1038/s41467-022-35519-4

29 Morabito, S. *et al.* Single-nucleus chromatin accessibility and transcriptomic characterization of Alzheimer's disease. *Nat Genet* **53**, 1143-1155 (2021). https://doi.org:10.1038/s41588-021-00894-z

30 Caglayan, E., Liu, Y. & Konopka, G. Neuronal ambient RNA contamination causes misinterpreted and masked cell types in brain single-nuclei datasets. *Neuron* (2022). https://doi.org:10.1016/j.neuron.2022.09.010

31 Huang, Y. *et al.* ELK4 exerts opposite roles in cytokine/chemokine production and degranulation in activated mast cells. *Front Immunol* **14**, 1171380 (2023). https://doi.org:10.3389/fimmu.2023.1171380

32 Bahl, E. *et al.* Using deep learning to quantify neuronal activation from single-cell and spatial transcriptomic data. *Nat Commun* **15**, 779 (2024). https://doi.org:10.1038/s41467-023-44503-5

33 Berto, S., Wang, G. Z., Germi, J., Lega, B. C. & Konopka, G. Human Genomic Signatures of Brain Oscillations During Memory Encoding. *Cereb Cortex* **28**, 1733-1748 (2018). https://doi.org:10.1093/cercor/bhx083

34 Badimon, A. *et al.* Negative feedback control of neuronal activity by microglia. *Nature* **586**, 417-423 (2020). https://doi.org:10.1038/s41586-020-2777-8

35 Laprell, L., Schulze, C., Brehme, M. L. & Oertner, T. G. The role of microglia membrane potential in chemotaxis. *J Neuroinflammation* **18**, 21 (2021). https://doi.org:10.1186/s12974-020-02048-0

36 Liu, Y. U. *et al.* Neuronal network activity controls microglial process surveillance in awake mice via norepinephrine signaling. *Nat Neurosci* **22**, 1771-1781 (2019). https://doi.org:10.1038/s41593-019-0511-3

37 Stowell, R. D. *et al.* Noradrenergic signaling in the wakeful state inhibits microglial surveillance and synaptic plasticity in the mouse visual cortex. *Nat Neurosci* **22**, 1782-1792 (2019). https://doi.org:10.1038/s41593-019-0514-0

38 Cheadle, L. *et al.* Sensory Experience Engages Microglia to Shape Neural Connectivity through a Non-Phagocytic Mechanism. *Neuron* **108**, 451-468 e459 (2020). https://doi.org:10.1016/j.neuron.2020.08.002

39 Estevao, C. *et al.* CCL4 induces inflammatory signalling and barrier disruption in the neurovascular endothelium. *Brain Behav Immun Health* **18**, 100370 (2021). https://doi.org:10.1016/j.bbih.2021.100370

40 Shen, Y. *et al.* CCR5 closes the temporal window for memory linking. *Nature* **606**, 146-152 (2022). https://doi.org:10.1038/s41586-022-04783-1

41 Chatterjee, S. *et al.* Endoplasmic reticulum chaperone genes encode effectors of long-term memory. *Sci Adv* **8**, eabm6063 (2022). https://doi.org:10.1126/sciadv.abm6063

42 Vanrobaeys, Y. *et al.* Mapping the spatial transcriptomic signature of the hippocampus during memory consolidation. *Nat Commun* **14**, 6100 (2023). https://doi.org:10.1038/s41467-023-41715-7

43 Rothe, T. *et al.* The Nuclear Receptor Nr4a1 Acts as a Microglia Rheostat and Serves as a Therapeutic Target in Autoimmune-Driven Central Nervous System Inflammation. *J Immunol* **198**, 3878-3885 (2017). https://doi.org:10.4049/jimmunol.1600638

44 Chiu, I. M. *et al.* A neurodegeneration-specific gene-expression signature of acutely isolated microglia from an amyotrophic lateral sclerosis mouse model. *Cell Rep* **4**, 385-401 (2013). https://doi.org:10.1016/j.celrep.2013.06.018

45 Olah, M. *et al.* Single cell RNA sequencing of human microglia uncovers a subset associated with Alzheimer's disease. *Nat Commun* **11**, 6129 (2020). https://doi.org:10.1038/s41467-020-19737-2

46 Sheng, R., Chen, C., Chen, H. & Yu, P. Repetitive transcranial magnetic stimulation for stroke rehabilitation: insights into the molecular and cellular mechanisms of neuroinflammation. *Front Immunol* **14**, 1197422 (2023). https://doi.org:10.3389/fimmu.2023.1197422

47 Heck, C. N. *et al.* Two-year seizure reduction in adults with medically intractable partial onset epilepsy treated with responsive neurostimulation: final results of the RNS System Pivotal trial. *Epilepsia* **55**, 432-441 (2014). https://doi.org:10.1111/epi.12534

48 Hammond, T. R. *et al.* Single-Cell RNA Sequencing of Microglia throughout the Mouse Lifespan and in the Injured Brain Reveals Complex Cell-State Changes. *Immunity* **50**, 253-271 e256 (2019). https://doi.org:10.1016/j.immuni.2018.11.004

49 Nott, A. *et al.* Brain cell type-specific enhancer-promoter interactome maps and disease-risk association. *Science* **366**, 1134-1139 (2019). https://doi.org:10.1126/science.aay0793

50 Hansson, A. C. & Fuxe, K. Time-course of immediate early gene expression in hippocampal subregions of adrenalectomized rats after acute corticosterone challenge. *Brain Res* **1215**, 1-10 (2008). https://doi.org:10.1016/j.brainres.2008.03.080

51 Cullinan, W. E., Herman, J. P., Battaglia, D. F., Akil, H. & Watson, S. J. Pattern and time course of immediate early gene expression in rat brain following acute stress. *Neuroscience* **64**, 477-505 (1995). https://doi.org:10.1016/0306-4522(94)00355-9

52 Dobin, A. *et al.* STAR: ultrafast universal RNA-seq aligner. *Bioinformatics* **29**, 15-21 (2013). https://doi.org:10.1093/bioinformatics/bts635

53 Liao, Y., Smyth, G. K. & Shi, W. featureCounts: an efficient general purpose program for assigning sequence reads to genomic features. *Bioinformatics* **30**, 923-930 (2014). https://doi.org:10.1093/bioinformatics/btt656

54 Risso, D., Schwartz, K., Sherlock, G. & Dudoit, S. GC-content normalization for RNA-Seq data. *BMC Bioinformatics* **12**, 480 (2011). https://doi.org:10.1186/1471-2105-12-480

55 Risso, D., Ngai, J., Speed, T. P. & Dudoit, S. Normalization of RNA-seq data using factor analysis of control genes or samples. *Nat Biotechnol* **32**, 896-902 (2014). https://doi.org:10.1038/nbt.2931

56 Peixoto, L. *et al.* How data analysis affects power, reproducibility and biological insight of RNA-seq studies in complex datasets. *Nucleic Acids Res* **43**, 7664-7674 (2015). https://doi.org:10.1093/nar/gkv736

862 57 Robinson, M. D., McCarthy, D. J. & Smyth, G. K. edgeR: a Bioconductor package
863 for differential expression analysis of digital gene expression data. *Bioinformatics*
864 **26**, 139-140 (2010). https://doi.org:10.1093/bioinformatics/btp616

865

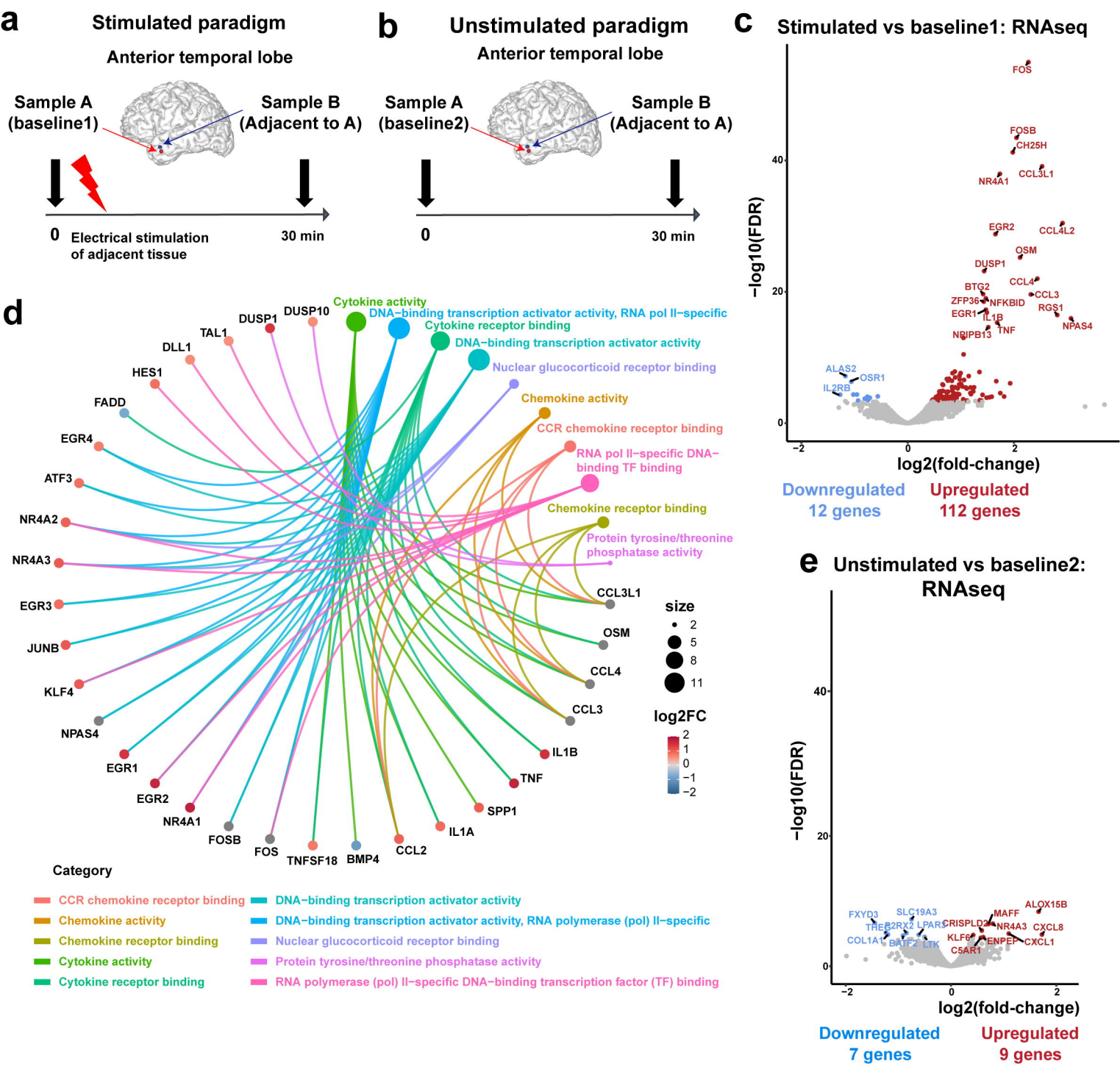
a
Stimulated paradigm
Anterior temporal lobe
Sample A
(baseline1)
Sample B
(Adjacent to A)
0
Electrical stimulation
of adjacent tissue
30 min
b
Unstimulated paradigm
Anterior temporal lobe
Sample A
(baseline2)
Sample B
(Adjacent to A)
0
30 min
c
Stimulated vs baseline1: RNAseq
−log10(FDR)
log2(fold-change)
FOS
FOSB
CH25H
CCL3L1
NR4A1
EGR2
CCL4L2
OSM
DUSP1
CCL4
BTG2
CCL3
ZFP36
NFKBID
RGS1
EGR1
IL1B
TNF
NPAS4
NR1PB13
ALAS2
OSR1
IL2RB
Downregulated
12 genes
Upregulated
112 genes
d
Cytokine activity
DNA−binding transcription activator activity, RNA pol II−specific
Cytokine receptor binding
DNA−binding transcription activator activity
Nuclear glucocorticoid receptor binding
Chemokine activity
CCR chemokine receptor binding
RNA pol II−specific DNA−binding TF binding
Chemokine receptor binding
Protein tyrosine/threonine phosphatase activity
DUSP1
DUSP10
TAL1
DLL1
HES1
FADD
EGR4
ATF3
NR4A2
NR4A3
EGR3
JUNB
KLF4
NPAS4
EGR1
EGR2
NR4A1
FOSB
FOS
TNFSF18
BMP4
CCL2
IL1A
SPP1
TNF
IL1B
CCL3
CCL4
OSM
CCL3L1
size
2
5
8
11
log2FC
2
1
0
−1
−2
Category
CCR chemokine receptor binding
Chemokine activity
Chemokine receptor binding
Cytokine activity
Cytokine receptor binding
DNA−binding transcription activator activity
DNA−binding transcription activator activity, RNA polymerase (pol) II−specific
Nuclear glucocorticoid receptor binding
Protein tyrosine/threonine phosphatase activity
RNA polymerase (pol) II−specific DNA−binding transcription factor (TF) binding
e
Unstimulated vs baseline2:
RNAseq
−log10(FDR)
log2(fold-change)
FXYD3
SLC19A3
MAFF
ALOX15B
TREM2
RXRA
LPAR5
CRISPLD2
NR4A3
CXCL8
COL1A1
KLF6
CXCL1
BATF2
LTK
C5AR1
Downregulated
7 genes
Upregulated
9 genes

Figure 1

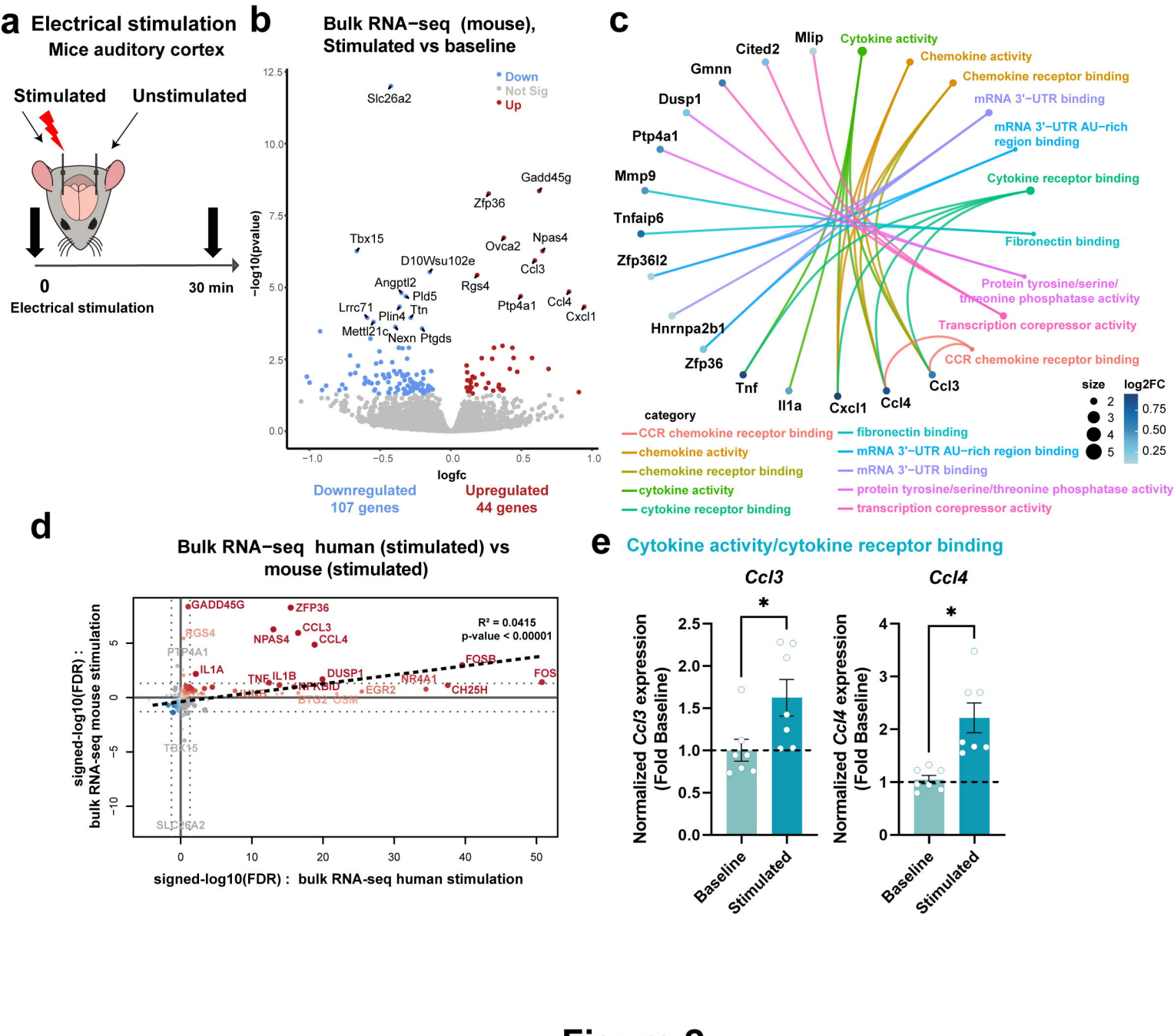
a
Electrical stimulation
Mice auditory cortex
Stimulated
Unstimulated
0
30 min
Electrical stimulation
b
Bulk RNA−seq (mouse),
Stimulated vs baseline
Down
Not Sig
Up
Slc26a2
Gadd45g
Zfp36
Tbx15
Ovca2
Npas4
D10Wsu102e
Ccl3
Angptl2
Rgs4
Pld5
Ptp4a1
Ccl4
Lrrc71
Ttn
Plin4
Cxcl1
Mettl21c
Nexn
Ptgds
−log10(pvalue)
logfc
Downregulated
107 genes
Upregulated
44 genes
c
Cytokine activity
Mlip
Cited2
Chemokine activity
Gmnn
Chemokine receptor binding
Dusp1
mRNA 3'−UTR binding
Ptp4a1
mRNA 3'−UTR AU−rich
region binding
Mmp9
Cytokine receptor binding
Tnfaip6
Fibronectin binding
Zfp36l2
Protein tyrosine/serine/
threonine phosphatase activity
Transcription corepressor activity
Hnrnpa2b1
CCR chemokine receptor binding
Zfp36
Tnf
Il1a
Cxcl1
Ccl4
Ccl3
size
log2FC
category
CCR chemokine receptor binding
chemokine activity
chemokine receptor binding
cytokine activity
cytokine receptor binding
fibronectin binding
mRNA 3'−UTR AU−rich region binding
mRNA 3'−UTR binding
protein tyrosine/serine/threonine phosphatase activity
transcription corepressor activity
d
Bulk RNA−seq human (stimulated) vs
mouse (stimulated)
R² = 0.0415
p-value < 0.00001
GADD45G
ZFP36
RGS4
CCL3
NPAS4
CCL4
PTP4A1
FOSB
IL1A
FOS
TNF
IL1B
DUSP1
NR4A1
EGR2
CH25H
TBX15
SLC26A2
signed-log10(FDR) :
bulk RNA-seq mouse stimulation
signed-log10(FDR) : bulk RNA-seq human stimulation
e
Cytokine activity/cytokine receptor binding
Ccl3
Ccl4
Normalized Ccl3 expression
(Fold Baseline)
Normalized Ccl4 expression
(Fold Baseline)
Baseline
Stimulated

Figure 2

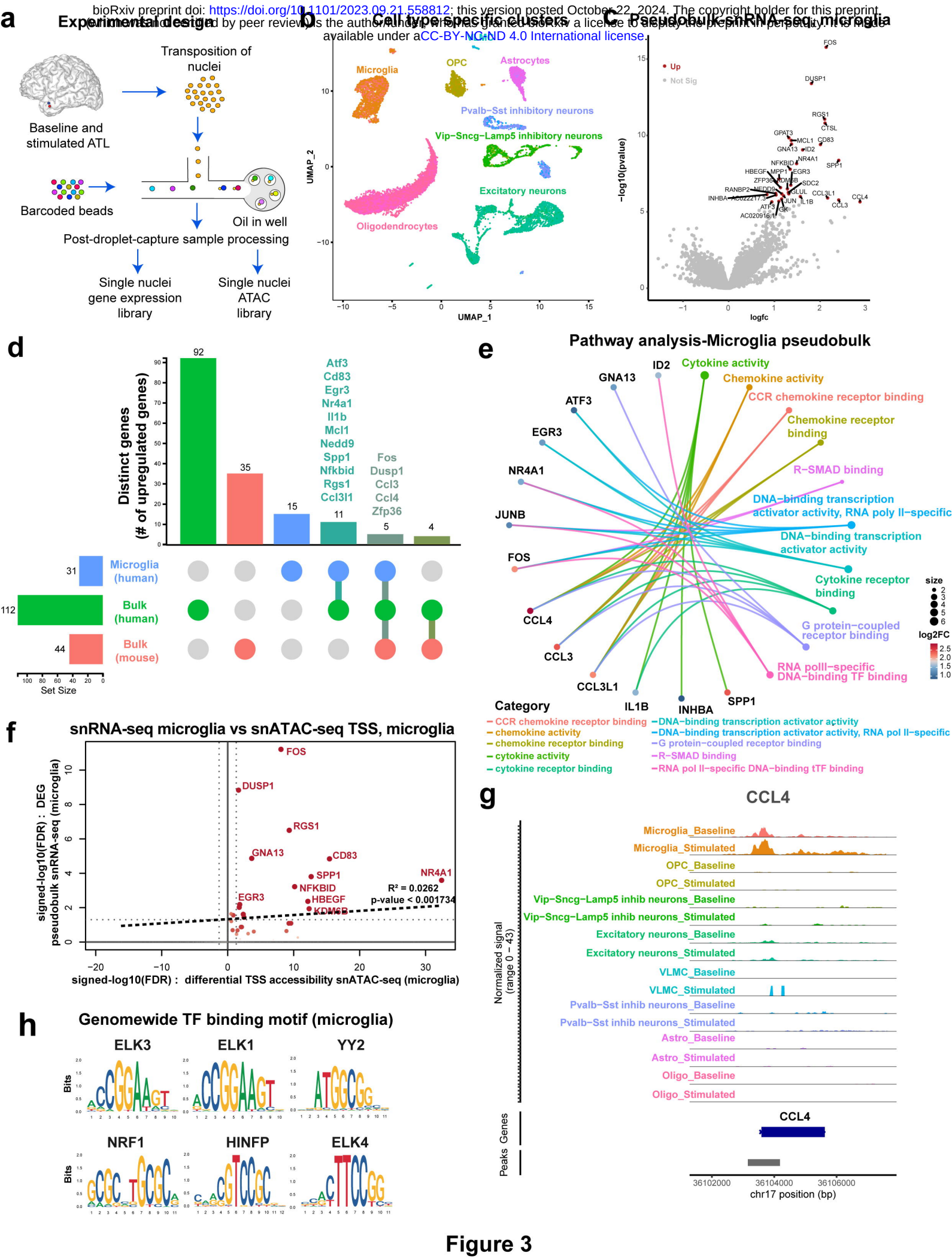

Figure 3

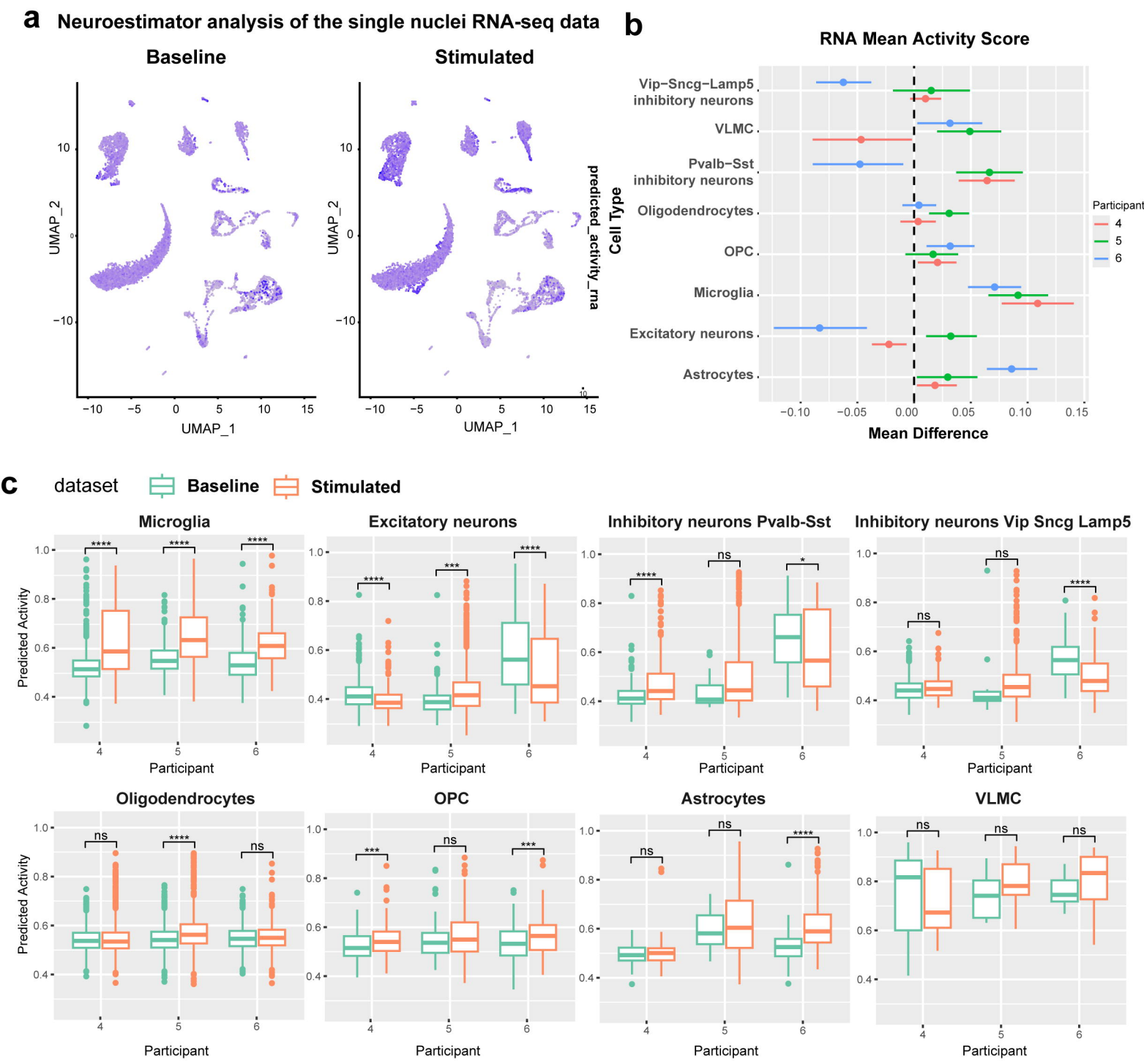
a
Neuroestimator analysis of the single nuclei RNA-seq data
Baseline
Stimulated
UMAP_2
UMAP_1
predicted_activity_rna
b
RNA Mean Activity Score
Cell Type
Vip−Sncg−Lamp5 inhibitory neurons
VLMC
Pvalb−Sst inhibitory neurons
Oligodendrocytes
OPC
Microglia
Excitatory neurons
Astrocytes
Participant
4
5
6
Mean Difference
c
dataset
Baseline
Stimulated
Microglia
Excitatory neurons
Inhibitory neurons Pvalb-Sst
Inhibitory neurons Vip Sncg Lamp5
Oligodendrocytes
OPC
Astrocytes
VLMC
Predicted Activity
Participant

Figure 4

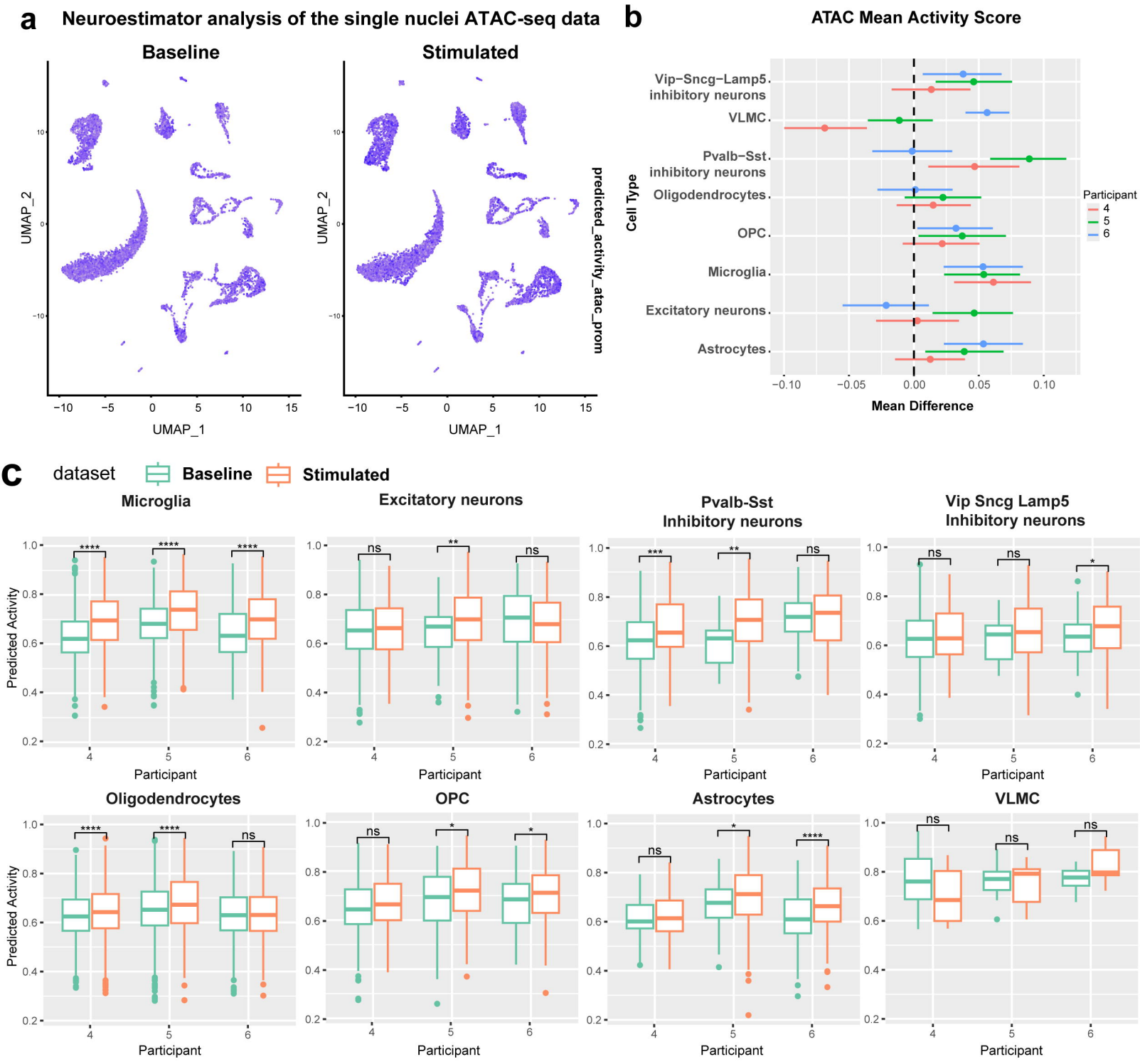
a
Neuroestimator analysis of the single nuclei ATAC-seq data
Baseline
Stimulated
UMAP_2
UMAP_1
predicted_activity_atac_prom
b
ATAC Mean Activity Score
Vip−Sncg−Lamp5 inhibitory neurons
VLMC
Pvalb−Sst inhibitory neurons
Oligodendrocytes
OPC
Microglia
Excitatory neurons
Astrocytes
Cell Type
Participant
4
5
6
−0.10
−0.05
0.00
0.05
0.10
Mean Difference
c
dataset
Baseline
Stimulated
Microglia
Excitatory neurons
Pvalb-Sst Inhibitory neurons
Vip Sncg Lamp5 Inhibitory neurons
Oligodendrocytes
OPC
Astrocytes
VLMC
Predicted Activity
Participant

Figure 5